

# Rigid-rod anion- $\pi$ slides for multiion hopping across lipid bilayers†‡

Virginie Gorteau, Guillaume Bollot, Jiri Mareda and Stefan Matile\*

Received 1st June 2007, Accepted 20th July 2007

First published as an Advance Article on the web 13th August 2007

DOI: 10.1039/b708337h

Shape-persistent oligo-*p*-phenylene-*N,N*-naphthalenediimide (O-NDI) rods are introduced as anion- $\pi$  slides for chloride-selective multiion hopping across lipid bilayers. Results from end-group engineering and covalent capture as O-NDI hairpins suggested that self-assembly into transmembrane O-NDI bundles is essential for activity. A halide topology VI ( $\text{Cl} > \text{F} > \text{Br} \sim \text{I}$ ,  $\text{Cl}/\text{Br} \sim \text{Cl}/\text{I} > 7$ ) implied strong anion binding along the anion- $\pi$  slides with relatively weak contributions from size exclusion ( $\text{F} \geq \text{OAc}$ ). Anomalous mole fraction effects (AMFE) supported the occurrence of multiion hopping along the  $\pi$ -acidic O-NDI rods. The existence of anion- $\pi$  interactions was corroborated by high-level *ab initio* and DFT calculations. The latter revealed positive NDI quadrupole moments far beyond the hexafluorobenzene standard. Computational studies further suggested that anion binding occurs at the confined,  $\pi$ -acidic edges of the sticky NDI surface and is influenced by the nature of the phenyl spacer between two NDIs. With regard to methods development, a detailed analysis of the detection of ion selectivity with the HPTS assay including AMFE in vesicles is provided.

## Introduction

Multiion hopping<sup>1,2</sup> enables biological ion channels to act selectively<sup>3,4</sup> and fast.<sup>1-14</sup> This is remarkable because the tight ion binding needed for high selectivity alone will slow down the transport of this recognized ion, whereas the “slippery” surfaces needed for fast diffusion are naturally not selective. The elegant solution of this dilemma is to align multiple binding sites next to each other for multiion hopping (Fig. 1). In the resting state, permanent occupation of some binding sites will hinder the passage of other ions, whereas complete occupation is unfavorable because of charge repulsion. In a channel with three active sites, the two peripheral sites will be filled and the central one will be empty (Fig. 1A). If now an ion approaches this channel to move across the membrane, the ion in the first active site will be repelled and move to the free central active site (Fig. 1B, a and b). The loading of the central binding site will repel the ion bound at the other periphery and cause its release (Fig. 1C, c and d). Overall, multiion hopping enables instantaneous release of strongly bound ions on one side of the membrane in response to anion binding on the other side.

The classical test for the existence of multiion hopping is the anomalous mole fraction effect (AMFE).<sup>1,2</sup> AMFE refers to lower than expected activity found with mixtures of ions compared to pure ions. Its occurrence indicates that permanent immobilization of the better binding ion to one single site of the channel is insufficient for significant transport of this ion (and may even hinder the transport of the less efficient ion). This, in turn, indicates that the occupation of multiple sites along the channel is required for efficient transport of the selected ion,

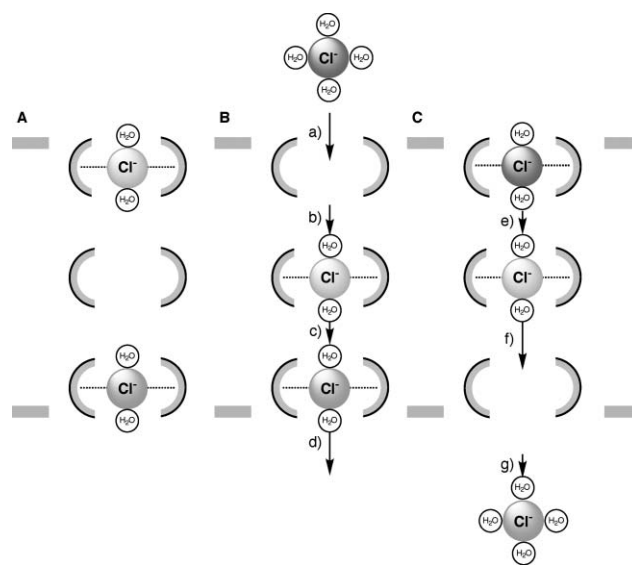


**Fig. 1** Multiion hopping solves the dilemma of ion channels to act in a fast and selective manner. (A) The resting state of a chloride channel with three aligned chloride binding sites may contain two permanently bound chlorides. (B) Repelled by the approaching external chloride (a), the chloride in the external binding site hops to the central site (b) to repel the chloride in the internal active site (c) to cause internal chloride release (d). (C) Repelled by the external chloride (e), the central chloride then hops to the internal site (f) to return to the resting state (A). Overall, the chloride bound externally and the chloride released internally are not the same.

*i.e.*, the existence of multiion hopping (Fig. 1). AMFE has been identified for many biological anion channels, including the cystic fibrosis transmembrane conductance regulator (CFTR) chloride channel,<sup>5-7</sup> the voltage-dependent chloride channel  $\text{ClC-0}$ ,<sup>8</sup>  $\text{Ca}^{2+}$ -activated chloride channels ( $\text{Cl}_{\text{Ca}}\text{Cs}$ ),<sup>9</sup> and so on.<sup>10</sup>

Multiion hopping has been confirmed on the structural level for cationic arginine clusters within the 16-stranded  $\beta$ -barrel of the

Department of Organic Chemistry, University of Geneva, Geneva, Switzerland. E-mail: stefan.matile@chiorg.unige.ch; Fax: +41 22 379 5123; Tel: +41 22 379 6523

† The HTML version of this article has been enhanced with colour images.

‡ Electronic supplementary information (ESI) available: Experimental details. See DOI: 10.1039/b708337h

porin Omp32<sup>11</sup> and three neutral, macrodipole-supported anion binding sites lined up within the complex  $\alpha$ -helix bundles of CICs.<sup>12</sup> The latter is reminiscent of the four neutral cation binding sites of potassium channels.<sup>13,14</sup>

Remarkably, the creation of synthetic channels, carriers and transporters with cation and anion selectivity from scratch is possible and has been demonstrated in many variations. For selected recent reviews, please see references 15–20. Cation selectivity became accessible with oligoether or oligocarbonyl arrays (including crown ethers) on scaffolds reaching from flexible alkyl chains<sup>17</sup> to more rigid dimeric steroids,<sup>21</sup> cucurbiturils,<sup>22</sup> *p*-octiphenyls,<sup>23</sup>  $\alpha$ -helices<sup>24</sup> and the  $\beta$ -helical gramicidin.<sup>25</sup> Interactions beyond multivalent oxygen ligands used to create cation selectivity include ion pairing along multiple carboxylate clusters<sup>26</sup> and counterion-mediated, pH-dependent inversion of the anion/cation selectivity of oligoarginine arrays.<sup>26</sup>

The more demanding anion selectivity has attracted recent attention because of the possible medicinal use as antibiotics and antitumor drugs, or to treat anion channelopathies, diseases that are caused by malfunction of anion channels such as CFTR, Cl<sub>Ca</sub>Cs, CICs, glycine and GABA receptors, and so on (cystic fibrosis, Best disease, Startle disease, Angelman syndrome, Bartter syndrome, myotonia, nephrolithiasis, osteopetrosis, and more).<sup>15,27–30</sup> Biomimetic approaches to anion selectivity have focused on fragments and derivatives of anion channel proteins<sup>27,28,31</sup> or natural products such as squalamine<sup>29,30</sup> and other cationic steroid antibiotics,<sup>32,33</sup> magainin and cationic peptide antibiotics,<sup>34–37</sup> or prodigiosin.<sup>38,39</sup> Anion recognition has been accomplished with amide or urea arrays on scaffolds such as macrocyclic (calixarene),<sup>40,41</sup> linear or branched<sup>42</sup> oligobenzyls or cholates.<sup>15,43,44</sup> Alternative to H-bonding approaches, ion pairing along arrays of ammonium or guanidinium cations has been successful on steroid,<sup>29,30,32,33</sup>  $\beta$ -peptide,<sup>34</sup> peptoid,<sup>35</sup> polynorbornene,<sup>36</sup> 1,3-polyphenyleneethynylene,<sup>37</sup> cyclodextrin,<sup>45</sup> or rigid-rod *p*-oligophenyl scaffolds.<sup>26,46</sup>

The use of synthetic organic chemistry to create new ion channels from scratch is attractive because of the possibility to expand the chemistry at work beyond the limitations of biology.<sup>15–20</sup> This has been accomplished for cation selectivity with fixed and flexible cation- $\pi$  interactions within calixarenes<sup>47</sup> and ligand-assembled *p*-septiphenyl rods (Fig. 2A),<sup>48</sup> respectively. As predicted theoretically,<sup>49</sup> flexible cation- $\pi$  interactions within supramolecular arene arrays were required to obtain the biologically relevant Eisenman IV selectivity sequence ( $K^+ > Rb^+ > Cs^+ > Na^+ \sim Li^+$ ). This sequence is difficult to obtain because it lies midway between the easily accessible Eisenman I, dominated by cation dehydration ( $Cs^+ > Rb^+ > K^+ > Na^+ > Li^+$ ), and Eisenman XI, dominated by cation binding in the channel ( $Li^+ > Na^+ > K^+ > Rb^+ > Cs^+$ ).<sup>3</sup>

Anion selectivity beyond anion/cation selectivity is usually described in anion selectivity sequences. Anion selectivity sequences report the preference of anion selective channels/transporters between different anions.<sup>3,49</sup> In the Eisenman theory,<sup>3</sup> ion selectivity sequences are thought to originate from a balance between dehydration penalty and energy gain from binding by the transporter. With direct correlation of cation radius and hydration energy, selectivity sequences can be plotted as Eisenman topologies, where ion selectivity is given as a function of the reciprocal ion radius. This naturally works best for group-one

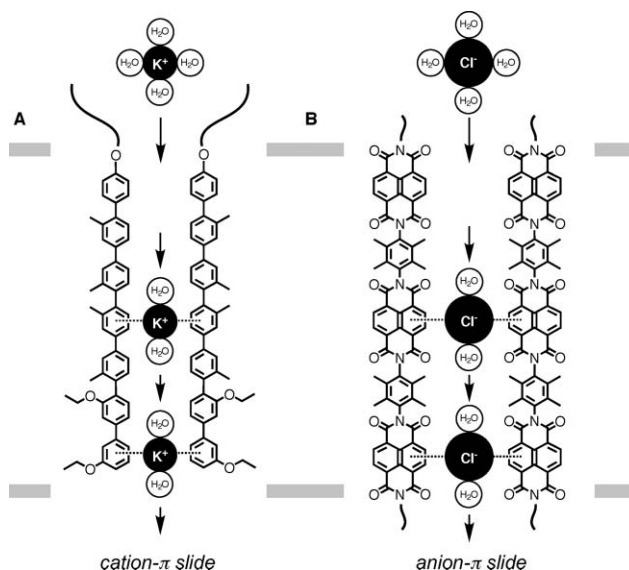


**Fig. 2** The concept of (A) cation- $\pi$  and (B) anion- $\pi$  slides for multiion hopping as outlined in Fig. 1. Cation- $\pi$  slides have been described previously,<sup>48</sup> the more demanding anion- $\pi$  slides are introduced in this report.

cations.<sup>3,48</sup> Application of the Eisenman theory to anions gives seven meaningful halide sequences.<sup>4</sup> One extreme is the very common “Wright–Diamond” sequence I ( $I^- > Br^- > Cl^- > F^-$ ). In halide I, also referred to as the Hofmeister series, selectivity is determined exclusively by the cost of anion dehydration. At the other end is the exceptionally rare halide VII ( $F^- > Cl^- > Br^- > I^-$ ). Here, selectivity is determined exclusively by anion binding to the channel. Intermediate selectivity sequences reflect a specific balance between dehydration penalty and binding in the channel. Anion selectivity sequences can be described as topologies. However, many mismatches of size (*e.g.*,  $OAc^- \gg F^-$ ) and hydration energy (*e.g.*,  $OAc^- \approx F^-$ ) limit the usefulness of selectivity topologies for anions beyond halides. The direct correlation of anion selectivity with hydration energy is often preferable for this reason.<sup>3,49</sup>

Complementary to the cation- $\pi$  interactions in the established rigid-rod cation- $\pi$  slides, the use of anion- $\pi$  interactions to create anion- $\pi$  slides is more challenging because little experimental support for this interaction is available in solution<sup>50,51</sup> despite quite extensive data from X-ray crystallography as well as from modeling.<sup>52–54</sup> Here,<sup>55</sup> we introduce rigid-rod molecules with multiple  $\pi$ -acidic naphthalenediimide (NDI)<sup>56–62</sup> binding sites along the transmembrane scaffold for this purpose (Fig. 2B). These shape-persistent oligo-*p*-phenylene-*N,N*-naphthalenediimide (O-NDI) rods are shown to preferably transport anions with relatively high hydration energy. Covalent capture as O-NDI hairpins and presumably unprecedented<sup>15–26</sup> AMFE are used to confirm strong binding and multiion hopping along transmembrane O-NDI  $\pi$ -slides as the origins of these attractive characteristics. We also report *ab initio* and DFT calculations of NDI and several model systems based on *N*-substituted NDIs. In particular, we have computed several complexes of chloride and bromide anions with these model systems. Parts of this study have been reported in the preliminary communication on this topic.<sup>55</sup>

## Results and discussion

### Design

The rigid O-NDI rods **1–5** were designed to explore the possibility of multiion hopping along anion- $\pi$  slides (Scheme 1 and Fig. 1 and 2). For this purpose, all rigid rods contain three  $\pi$ -acidic NDI binding sites along their scaffold. The phenyl spacers, with their planes perpendicular to the NDI planes, were fully methylated to assure high solubility. Moreover, these methyls should also increase the overall quadrupole moment of the O-NDI rod to better attract anions and confine the  $\pi$ -acidic edges of the NDI surface to possibly match the diameter of chloride and possibly weaken anion- $\pi$  interactions with the larger bromide or iodide (see section on molecular modeling). To ensure a transmembrane rod orientation, we made sure that the overall length of the rigid O-NDI rods (3.4 nm) matched the thickness of the hydrophobic core of EYPC bilayer membranes.<sup>63,64</sup>

The O-NDI rods **1–3** have differently charged termini. Rod **1** is uncharged, rod **2** has one cationic and one uncharged terminus, and rod **3** has two cationic termini. The neutral O-NDI hairpin **4** corresponds to a dimeric bundle of neutral rods **1**. The dicationic O-NDI hairpin **5** corresponds to a parallel dimer of rods **2** with one cationic and one neutral terminus. This series was prepared to probe the importance of terminal charges for activity<sup>23,24</sup> and to explore the dependence of anion selectivity on the lateral proximity of self-assembled transmembrane rods.<sup>48</sup>

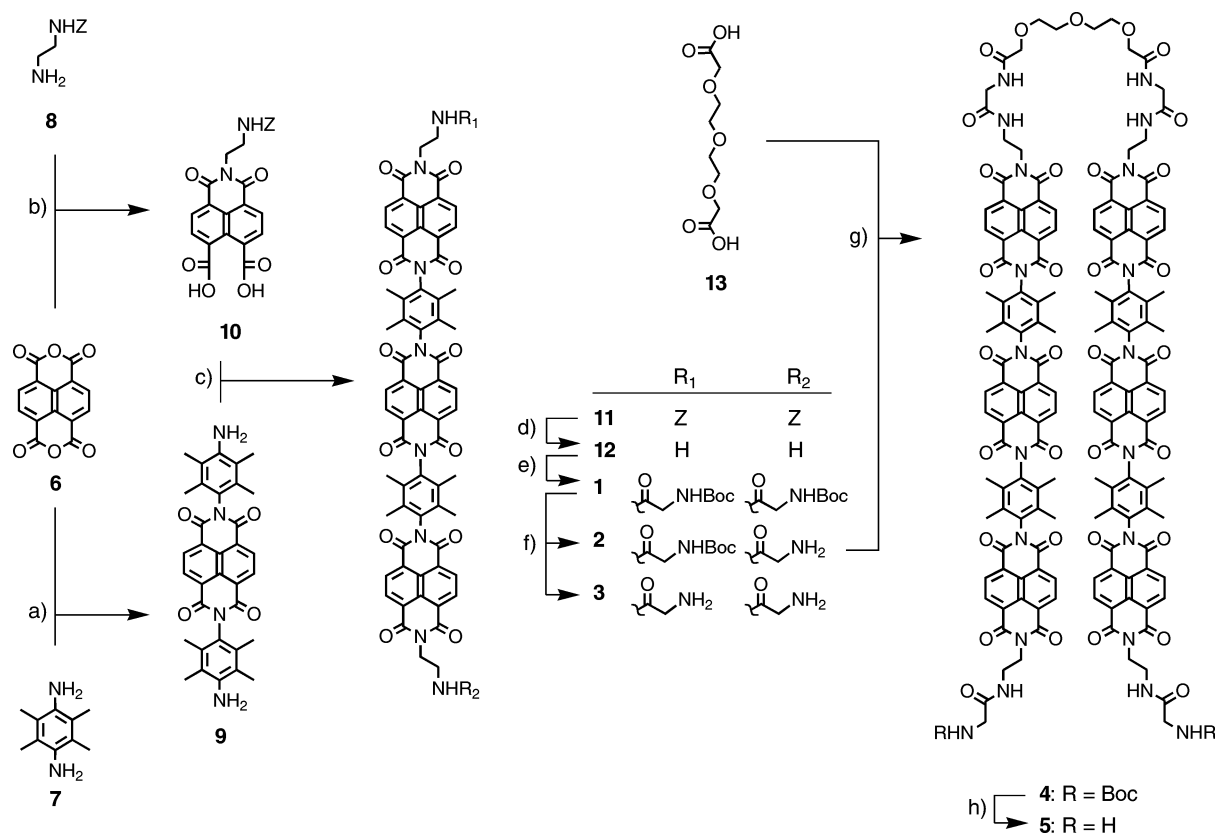
### Synthesis

Rigid O-NDI rods **1–5** were prepared from naphthalenedianhydride **6**, aryl diamine **7** and alkyl amine **8** (Scheme 1). Treatment of dianhydride **6** with excess diamine **7** gave the central NDI module **9**. Controlled introduction of amine **8** provided the imide terminus **10**. Coupling of imide termini **10** and central module **9** already afforded the desired rigid-rod scaffold.

Modifications of the O-NDI termini were initiated with the removal of the Z-protection of rod **11**. Attempts to isolate the asymmetric monoamine intermediate under mild conditions failed. The obtained diamine **12** was thus elongated with Boc-protected glycine. "Ultramild" partial Boc-removal from the obtained rod **1** gave a roughly statistical mixture of rods **1**, **2** and **3**, which were readily isolated and purified. Availability of the asymmetric rod **2** was essential to prepare O-NDI hairpins. Coupling with diacid **13** gave the neutral hairpin **4**, deprotection with TFA the dicationic hairpin **5**.

### Activity

The activity of rigid-rod anion- $\pi$  slides **1–5** was determined in egg yolk phosphatidylcholine large unilamellar vesicles (EYPC LUVs) that were loaded with the pH-sensitive fluorescent probe 8-hydroxy-1,3,6-pyrenetrisulfonate (HPTS) at neutral pH.<sup>23,46,48,55,65</sup> Then, a pH gradient  $\Delta\text{pH} = 0.9$  was applied with a base pulse, and the changes in HPTS emission were recorded as a function of time



**Scheme 1** Synthesis of rigid-rod anion- $\pi$  slides **1–5**. (a) *N,N*-Dimethylacetamide, 135 °C, 12 h, 90%. (b) 1. H<sub>2</sub>O, pH 6.4, reflux; 2. AcOH, 88% (overall). (c) *N,N*-Dimethylacetamide, 135 °C, 12 h, 57%. (d) TFA, 50 °C, 2 h, 61%. (e) Boc-Gly-OH, HBTU, TEA, rt, 2 h, 54%. (f) 2% TFA, CH<sub>2</sub>Cl<sub>2</sub>, rt, 50 min, 64% **2**, 30% **3** (conversion yield). (g) 1. **13**, oxalylchloride, 2. *N*-hydroxysuccinimide, 3. **2**, TEA, 0 → 20 °C, 20 min, 36%. (h) TFA, rt, 2 h, 79%.

(Fig. 3). Rods 1–5 were added next, and the velocity of the decay of the pH gradient was monitored continuously following the change in HPTS emission. At the end of each experiment, an excess of gramicidin A, melittin, or triton X-100 was added for calibration. Each experiment was recorded in two channels at different HPTS excitation to ratiometrically eliminate eventual effects from origins other than change in pH. Each experiment was repeated without rods, and the normalized background traces were subtracted to unambiguously extract the changes caused by rigid-rod anion- $\pi$  slides. Fig. 3 shows representative curves for the activity of rod 1 at different concentrations after the elimination of all unrelated effects by background subtraction.

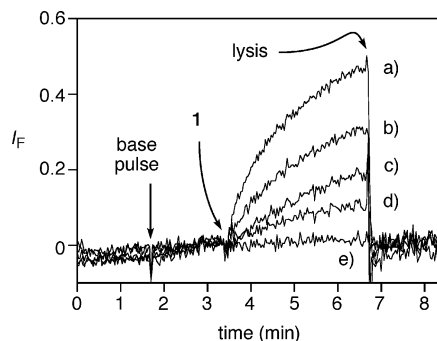


**Fig. 3** Dependence of activity on the concentration of rigid O-NDI rod 1. Fractional HPTS emission intensity  $I_F$  ( $\lambda_{\text{ex}}$  450 nm,  $\lambda_{\text{em}}$  510 nm) is shown during the addition of first NaOH (20  $\mu\text{l}$ , 0.5 M), then rod 1 (0.15 (a), 0.375 (b), 1.5 (c), 2.5 (d) and 15  $\mu\text{M}$  (e) final concentration) to EYPC-LUVs $\supset$ HPTS (1 mM HPTS, 10 mM HEPES, 100 mM NaCl, pH 7.0, 25  $^{\circ}\text{C}$ , calibrated by final addition of excess gramicidin A or triton X-100). Negative controls without rod were subtracted after calibration.

### Hill plots

The HPTS assay was used to determine the dependence of the activity on the concentration of rods 1–5. The highest activity was found for the singly charged O-NDI rod 2 (Fig. 4,  $\circ$ ), followed by the uncharged rod 1 (Fig. 4,  $\blacksquare$ ), whereas dication 3 was the least active of all monomeric rods (Fig. 4, X).

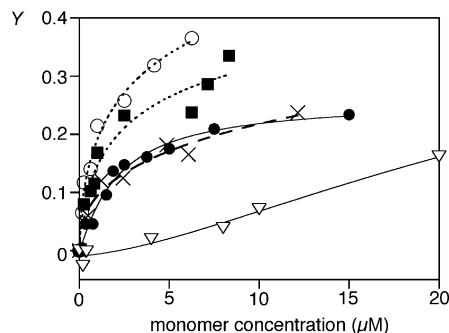


**Fig. 4** Hill plot of rods 1 ( $\blacksquare$ ), 2 ( $\circ$ ), 3 (X), 4 ( $\bullet$ ) and 5 ( $\nabla$ ). The dependence of the fractional activity  $Y$  on monomer concentration was determined in EYPC-LUVs $\supset$ HPTS as specified in Fig. 3. The term fractional activity  $Y$  is used to compare fractional HPTS emissions  $I_F$  at a given time (here 200 s) after the start of the transport experiment, compare Fig. 3 for changes of  $I_F$  with time.

These trends supported the existence of an active structure with membrane-spanning rods. The highest activity for rod 2 with one charged terminus implied that sufficient water solubility to reach the membrane on the one hand and favored partitioning and translocation of the hydrophobic terminus to adapt a transmembrane active structure on the other hand are both important for function. Insufficient water solubility with partial precipitation before reaching the membrane could account for the decreasing activity of rod 1 without charged termini.<sup>66</sup> However, further reduced activity of rod 3 with two charged termini and thus unproblematic solubility in water identified the translocation of one rod terminus, *i.e.*, transmembrane rod orientation, as most critical for activity.<sup>23</sup>

The overall disappointing activities of O-NDI hairpins 4 (Fig. 4,  $\bullet$ ) and 5 (Fig. 4,  $\nabla$ ) were in agreement with these interpretations in support of transmembrane active structures. The activity of the neutral O-NDI hairpin 4 was a bit weaker than that of neutral O-NDI rod 1, suggesting that the solubility in water may have further decreased. The activity of doubly charged hairpin 5 was exceptionally weak. This finding was somewhat surprising because hairpin 5 could span the membrane with both positive charges resting at the outer membrane–water interface as with the most active monocationic rod 2 (Scheme 1). The poor activity of dicationic hairpin 5 may thus indicate that the translocation of the oligoethyleneglycol loop across the membrane to adapt a transmembrane hairpin with external charges is unfavorable. Alternative explanations include self-assembly of dicationic O-NDI (bola)amphiphiles 5 into micelles or vesicles rather than binding to the lipid bilayer, and so on.

Pseudo-linear behavior at low concentrations and saturation behavior at high concentrations made Hill analysis of the Hill plots of rods 1–4 rather unrevealing.<sup>65–68</sup> The latter indicated interference from increasing rod precipitation at increasing concentrations (rather than partitioning into the membrane). The former indicated either a monomeric active structure or, more likely (see below), the exergonic self-assembly into thermodynamically stable active supramolecules, *i.e.*, supramolecular anion- $\pi$  slides (Fig. 2).

### Anion selectivity

The decay of a pH gradient measured in the HPTS assay can occur by facilitated cation ( $\text{H}^+/\text{M}^{n+}$ ) or anion exchange ( $\text{OH}^-/\text{X}^{n-}$ ).<sup>65</sup> The activity of anion- $\pi$  slide 1 did not change in response to the replacement of external  $\text{Na}^+$  by  $\text{K}^+$ ,  $\text{Rb}^+$  or  $\text{Cs}^+$ . This insensitivity to external cation exchange suggested that rigid O-NDI rod 1 does not transport cations.<sup>55</sup> Anion- $\pi$  slide 1, however, did respond to external anion exchange (Fig. 5), implying the selective transport of anions rather than cations. The complementary sensitivity of cation- $\pi$  slides (Fig. 2A) to cation and insensitivity to anion exchange has been demonstrated previously.<sup>48</sup>

The different activity of O-NDI rod 1 found with different external anions provided access to anion selectivity sequences (Fig. 5). To really understand ion selectivity sequences obtained from the HPTS assay, a careful analysis of all situations was unavoidable.<sup>65,69</sup> The situation in symmetric NaCl was unproblematic (Scheme 2a). Application of a base pulse before the  $\pi$ -slide will create an additional pH gradient (Scheme 2b). Addition of an anion exchanger such as rod 1 will then initiate transmembrane  $\text{Cl}^-/\text{Cl}^-$  and  $\text{Cl}^-/\text{OH}^-$  antiport (Scheme 2c).

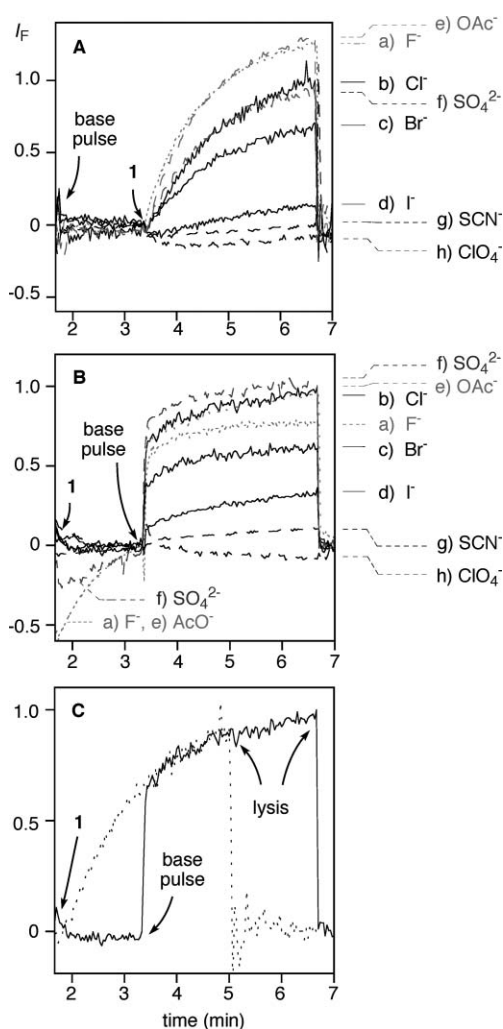
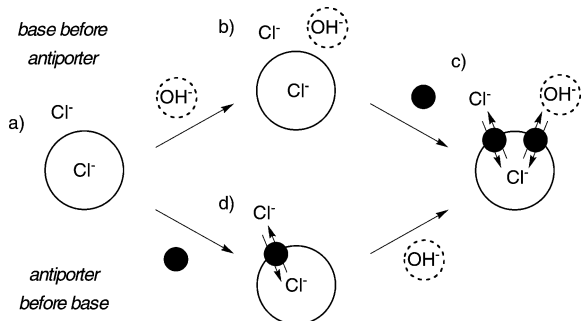


**Fig. 5** Dependence of the anion selectivity of rod **1** in vesicles with internal  $\text{Cl}^-$  on the sequence of addition. Fractional emission  $I_F$  (with respect to  $\text{Cl}^-$ ) during the addition of either (A) first NaOH (20  $\mu\text{l}$  0.5 M) and then rod **1** (1.5  $\mu\text{M}$  final concentration) or (B) first **1** and then NaOH to EYPC-LUVs>HPTS exposed to varied external anions (sodium salts, conditions as in Fig. 3), with final lysis for calibration. (C) Overlay of curves b (with NaCl) from A (dotted) and B (solid).



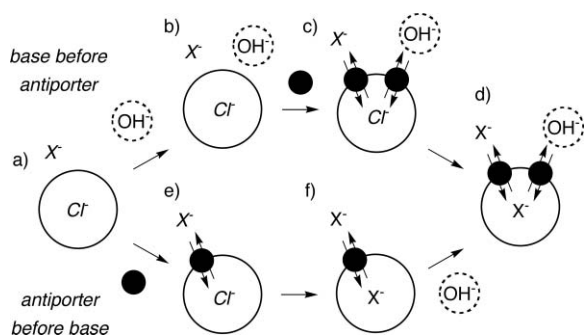
**Scheme 2** The HPTS assay for anion antiporters in symmetric NaCl is independent of the sequence of addition: base pulse before antiporter addition (top) and antiporter addition before base pulse (bottom) provide access to the detection of  $\text{Cl}^-/\text{OH}^-$  antiport as increase in intravesicular pH (vesicles = solid circles; antiporter = filled circles; added base = dashed circles, see text for discussion).

The former is unproductive and invisible, the latter dissipates the applied pH gradient and is reported by intravesicular pH probes as increase in pH (Fig 5Ab). Rod addition before base pulse will immediately turn on the unproductive and invisible  $\text{Cl}^-/\text{Cl}^-$  antiport, together with similarly unproductive  $\text{OH}^-/\text{Cl}^-$  antiport,  $\text{Cl}^-/\text{OH}^-$  antiport and  $\text{OH}^-/\text{OH}^-$  antiport (Scheme 2d). Productive  $\text{Cl}^-/\text{OH}^-$  antiport will occur in response to a base pulse, and  $\text{OH}^-$  influx is detectable as a biphasic increase in pH (Scheme 2c, Fig. 5Bb). With identical final systems, the apparent activities are thus expected to be independent of the sequence of addition (Scheme 2c). However, slide addition before base pulse decouples the slow formation of the active structure (partitioning, intervesicular transfer, translocation, and so on) from the much faster actual anion exchange. For this reason, the observed initial rate is much faster for slide addition before base pulse than base pulse before slide addition (Fig. 5C). After this initial fast anion exchange along a high number of already preformed slides, the kinetics for slide before base and base before slide addition were perfectly superimposable.

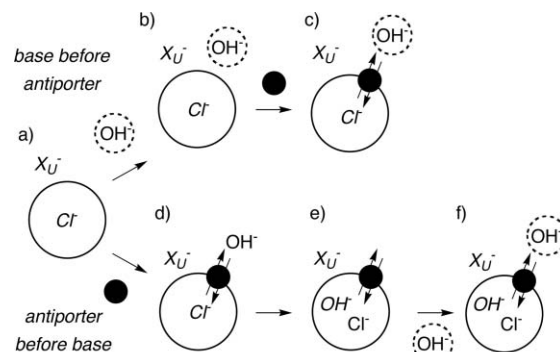
The reason why the two curves in Fig. 5C are so nicely superimposable after the second base pulse may not be easily appreciated. To do so, it may be best to assume intervesicular transfer as the rate limiting process of slide formation. The observed fractional activity would then reflect, at any given time, the number of vesicles containing  $\pi$ -slides. This number will steadily increase after slide addition, independent of the time the base pulse is applied (Fig. 5C). This increasing number of  $\pi$ -slide-rich vesicles is naturally invisible without base pulse (Fig. 5C, solid). Application of the base pulse after slide addition will then cause an instantaneous pH jump corresponding to the number of  $\pi$ -slide-rich vesicles and afterwards continue to rise slowly following the kinetics of intervesicular slide transfer. We reiterate all changes in HPTS emission found in the HPTS assay including the initial jump after base pulse in the presence of slide **1** could originate not only from rapid  $\text{OH}^-/\text{X}^-$  antiport but also from HPTS efflux or cation antiport. The occurrence of  $\text{OH}^-/\text{X}^-$  antiport was revealed by the dependence of all changes, including this initial jump (Fig. 5B), on the nature of the extravesicular anion  $\text{X}^{n-}$ .

To determine anion selectivity sequences, isoosmolar external  $\text{Cl}^- \rightarrow \text{X}^-$  exchange was used.<sup>65,69</sup> This exchange produces transmembrane  $\text{Cl}^-/\text{X}^-$  gradients that significantly complicate the situation. Different processes are expected to occur with external non-basic anions that are transported by the slide ( $\text{X}^-$ , Scheme 3), with weakly basic anions ( $\text{X}_B^-$ , Scheme 4), and with unrecognized anions that are not transported at all by the slide ( $\text{X}_U^-$ , Scheme 5).

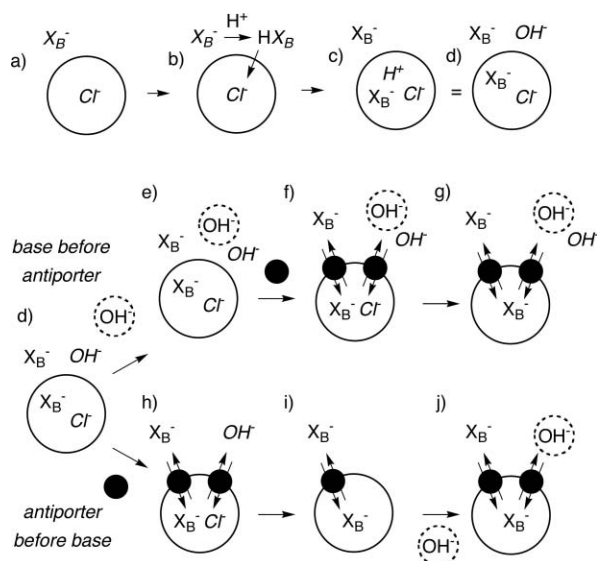
HPTS assays for anion selectivity with non-basic anions  $\text{X}^-$  that are transported by the slide of interest provide the following information (Scheme 3). Base pulse before slide addition will add a pH gradient to the  $\text{Cl}^-/\text{X}^-$  gradients (Scheme 3b). Slide addition will then turn on  $\text{Cl}^-/\text{X}^-$  and  $\text{Cl}^-/\text{OH}^-$  antiport (Scheme 3c). With the concentrations of  $\text{X}^-$  (100 mM) more than three orders of magnitude higher than that of  $\text{OH}^-$  (pH  $\sim$  8),  $\text{Cl}^-/\text{X}^-$  antiport will be much faster than  $\text{Cl}^-/\text{OH}^-$  antiport, even at high  $\text{OH}^- > \text{X}^-$  selectivity. The  $\text{Cl}^-/\text{X}^-$  gradients will thus disappear well before the occurrence of significant  $\text{OH}^-$  transport. With overall much higher concentration of  $\text{X}^-$  (extravesicular exceeds intravesicular volume by far),  $\text{Cl}^-$  concentrations are negligible in transmembrane equilibrium. The process reported in the HPTS



**Scheme 3** HPTS assay for anion selectivity with non-basic anions  $X^-$ . With internal NaCl and external NaX,  $X^-/OH^-$  antiport is reported as increase in intravesicular pH (d), independent of sequence of addition, *i.e.*, base pulse before antiporter addition (top) and antiporter addition before base pulse (bottom; vesicles = empty circles; antiporter = filled circles; added base = dashed circles, other anion gradients are in italics, see text for discussion).



**Scheme 5** HPTS assay for anion selectivity with unrecognized anions  $X_U^-$ , *i.e.*, anions that are not transported by the antiporter of interest. In this case,  $Cl^-/OH^-$  antiport is reported independent of sequence of addition (c, f). Unrecognized anions  $X_U^-$  can be identified by  $OH^-$  influx without applied pH gradient (d). The influence of the additional  $Cl^-$  (c) or  $OH^-$  gradients (e, f) appears less important.



**Scheme 4** HPTS assay for anion selectivity with weakly basic anions  $X_B^-$ .  $HX_B$  influx before base pulse and antiporter addition (top) gives overestimates of  $X_B^-/OH^-$  antiport for base pulse before antiporter addition (middle) but comparable data on  $X_B^-/OH^-$  antiport for antiporter addition before base pulse (bottom).  $X_B^-$  are identified by low initial emission (c, d) that disappears in response to antiporter addition without base pulse (h, i).

assay for anion selectivity is thus  $X^-/OH^-$  antiport (Scheme 3d). Addition of the transporter before the base pulse leads to the same situation (Scheme 3e and f). Independence of activities on sequence of addition found with rigid O-NDI rod **1** for  $Cl^-/OH^-$ ,  $Br^-/OH^-$  and  $I^-/OH^-$  antiport was in agreement with this interpretation, anion basicity is thought to account for the dependence of  $F^-/OH^-$  antiport on sequence of addition (Fig. 5).

The initial HPTS emission in vesicles with weakly basic external anions  $X_B^-$  such as  $F^-$  and  $OAc^-$  was much weaker than that with non-basic anions  $X^-$  (Fig. 5Ba). We interpreted this phenomenon as passive influx of  $HX_B$  in response to external  $Cl^- \rightarrow X_B^-$  exchange (Scheme 4). This internal acidification was observed for weak bases such as  $F^-$  and  $OAc^-$  but not for non-basic anions such as  $Br^-$ ,  $I^-$  or  $ClO_4^-$  (Fig. 5a and 5e;  $SO_4^{2-}$  is special, see Scheme 5).

Addition of rod **1** to HF-acidified vesicles naturally removed this HF-mediated pH gradient and made the HPTS emission return to normal before application of the base pulse (Fig. 5Ba and 5Be).

The consequences of the internal acidification with weakly basic anions  $X_B^-$  on HPTS assays for anion selectivity were dependent of the sequence of addition (Scheme 4). With the base pulse applied first, the final effective pH gradient with weakly basic anions  $X_B^-$  (Scheme 4g) is larger than with non-basic anions  $X^-$  (Scheme 3d). With the antiporter added first, however, the final effective pH gradients with weakly basic anions  $X_B^-$  (Scheme 4j) and non-basic anions  $X^-$  (Scheme 3d) are identical. Results on ion selectivity with weakly and non-basic anions  $X_B^-$  and  $X^-$  obtained by slide addition before base pulse should thus be directly comparable (Fig. 5B), whereas results obtained by base pulse before slide addition may give activities for weakly basic anions  $X_B^-$  that appear higher than they are in reality (Fig. 5A; please consult the ESI† for a more detailed discussion of the  $X_B^-$  anomaly).

Another class of anions that required special attention were unrecognized anions  $X_U^-$ , *i.e.*, anions that are not transported by the anion antiporter (Scheme 5). In this case, addition of first base and then slide will create a system where the internal  $Cl^-$  is not exchanged by the unrecognized anion  $X_U^-$  (Scheme 5a–c). Activities found in the HPTS assay will thus report on  $Cl^-/OH^-$  antiport. Often, this situation can be clarified by reversal of the sequence of addition (Scheme 5d–f).  $Cl^-/X_U^-$  antiport excluded,  $Cl^-/OH^-$  antiport could occur (Scheme 5d). The resulting increase of intravesicular pH is detectable in the HPTS assay (Scheme 5e). This formal proton pumping was observed with slide **1** for  $SO_4^{2-}$ , although the effect was relatively weak (Fig. 5Bf; much stronger proton pumping was confirmed to occur with other transporters in the presence of  $SO_4^{2-}$  and also  $NO_3^-$  and  $ClO_4^-$ ).<sup>70</sup> The activities found for rod **1** with external  $SO_4^{2-}$  and  $Cl^-$  were indeed identical. They thus report both on  $Cl^-/OH^-$  antiport and should not be confused with  $SO_4^{2-}$  selectivity (Fig. 5B, b and f).

Taken together, the lessons learned concerning HPTS assays for anion selectivity are as follows. (a) Activities obtained by external exchange with non-basic anions  $X^-$  report directly on  $X^-/OH^-$  antiport and are independent on sequence of addition

(Scheme 2 and 3). (b)  $X_B^-$  anomaly: activities obtained by external exchange with weakly basic anions  $X_B^-$  such as  $F^-$  or  $OAc^-$  give results comparable with non-basic anions  $X^-$  only if the antiporter is added before the base (Fig. 5Ba and 5Be, base pulse before antiporter addition gives overestimates, Scheme 4, Fig. 5Aa and 5Ae). (c)  $X_U^-$  anomaly: results with unrecognized anions  $X_U^-$  report on  $Cl^-/OH^-$  antiport (Scheme 5, here  $SO_4^{2-}$ , Fig. 5Bf). We caution that this analysis is necessarily incomplete, blockage by competitive and permeant anions, for example, is not considered.<sup>9,71,72</sup>

With these considerations in mind, the anion selectivity sequences of O-NDI rods were determined from the dependence of the fractional activity  $Y$  relative to  $Cl^-$  on the reciprocal anion radius (Fig. 6) or the anion hydration energy (Fig. 7). Experimental evidence suggested that permeability ratios from Goldman–Hodgkin–Katz analysis of planar bilayer conductance experiments and results on ion selectivity from the HPTS assay are directly comparable.<sup>46</sup> The activities of O-NDI rod **1** found in HPTS assays decreased with increasing halide radius (Fig. 5A and 6A, ■). The uncertainty in the measure of the transport of the  $F^-$  made it generally difficult to discriminate between VII ( $F^- > Cl^- > Br^- > I^-$ ), halide VI ( $Cl^- > F^- > Br^- > I^-$ ) and halide V selectivity ( $Cl^- > Br^- > F^- > I^-$ ).<sup>55</sup> However, all these exceptionally rare<sup>1–10</sup> halide topologies are opposite to the ubiquitous, dehydration-dominated Hofmeister series or halide I. According to the Eisenman theory,<sup>3,4</sup> this finding implied exceptionally strong anion binding along the rigid-rod O-NDI  $\pi$ -slide **1**. This interpretation was supported by the results for acetate. This weakly basic anion is a classical probe<sup>9</sup> because it is large but still difficult to dehydrate. High activity found for  $OAc^-/OH^-$  exchange excluded size exclusion effects (Fig. 6A, ■) and confirmed strong anion binding to slide **1** as origin of selectivity (Fig. 7A, ■).

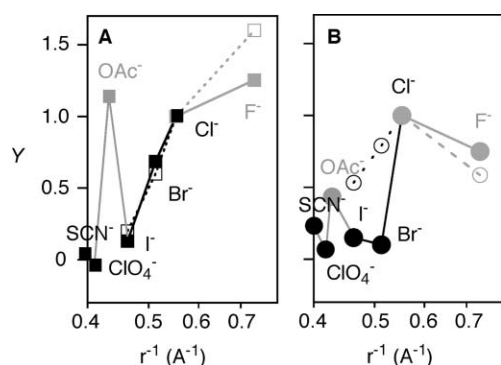


**Fig. 6** Anion selectivity of rods **1** (A, ■, □), **2** (B, ○) and **4** (B, ●). Fractional activity  $Y$  (relative to  $Cl^-$ ) as a function of the reciprocal anion radius was determined with the HPTS assay with initial intravesicular  $Cl^-$  (■, ○, ●) and  $Br^-$  (□). Data for  $F^-$  and  $OAc^-$  are in grey to highlight that they represent systematic overestimates (Scheme 4). For original data, see Fig. 5A, 8A and 8B (rod addition after base pulse).

The dependence of the effective selectivity sequence determined in the HPTS assay on the initial intravesicular anion was determined next. For this purpose, internal  $Cl^-$  was replaced by internal  $Br^-$ , and anion selectivity was determined by external anion exchange (Fig. 8A). The effective selectivity sequence found with internal  $Br^-$  was nearly identical with the selectivity sequence

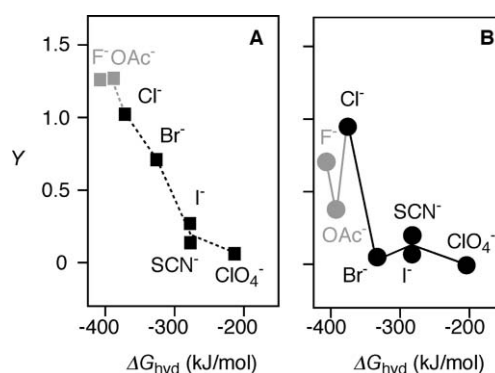


**Fig. 7** Anion selectivity of rods **1** (A, ■) and **4** (B, ●). Fractional activity  $Y$  (relative to  $Cl^-$ ) as a function of the anion hydration energy was determined with the HPTS assay with initial intravesicular  $Cl^-$ . Data for  $F^-$  and  $OAc^-$  are in grey to highlight that they represent systematic overestimates (Scheme 4). For original data, see Fig. 5A and 8B (rod addition after base pulse).

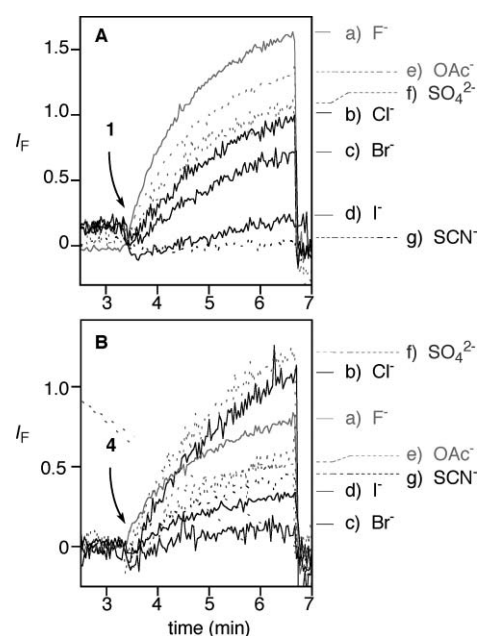


**Fig. 8** Anion selectivity of (A) rod **1** in vesicles with internal  $Br^-$  and (B) rod **4** in vesicles with internal  $Cl^-$ . Fractional emission  $I_F$  (relative to  $Cl^-$ ) during the addition of NaOH (20  $\mu$ l 0.5 M) and then **1** (1.5  $\mu$ M) or **4** (2.5  $\mu$ M) to EYPC-LUVs $\Delta$ HPTS exposed to varied external anions (sodium salts, as in Fig. 3).

found with internal  $Cl^-$  (Fig. 6A, ■ vs. □). Particularly noteworthy was the independence of  $Cl^- > Br^-$  selectivity on internal  $Cl^- \rightarrow Br^-$  exchange. It supported the interpretation that the presence or the absence of initial transmembrane  $Cl^-$  and  $Br^-$  gradients has little influence on the velocity of  $OH^-/X^-$  exchange reported in the HPTS assay (Scheme 3). Specifically, this finding supported that, after addition of rod **1**, the replacement of internal  $Cl^-$  and  $Br^-$  by external  $X^-$  is much faster than  $OH^-/X^-$  exchange because the concentration of  $X^-$  exceeds that of  $OH^-$  and  $Cl^-$  by far.

The anion selectivity of the most active cationic  $\pi$ -slide **2** with one cationic terminus was determined as described in Fig. 5A for rod **1** (Fig. 6B, ○).<sup>55</sup> The selectivity topology revealed decreasing

anion selectivity of cationic rod **2** ( $\text{Cl}^-/\text{I}^- = 1.9$ ) compared to neutral rod **1** ( $\text{Cl}^-/\text{I}^- = 7.6$ , Fig. 6A, ■ vs. Fig. 6B, ○).

Contrary to its poor activity (Fig. 4), the neutral O-NDI hairpin **4** exhibited excellent anion selectivity (Fig. 8B). Compared to the selectivity sequence of the neutral O-NDI monomer **1** determined under identical conditions (Fig. 5A), the reduced activity found with  $\text{F}^-$ ,  $\text{OAc}^-$  as well as  $\text{Br}^-$  was most intriguing (**1**:  $\text{Cl}^-/\text{Br}^- = 1.5$ , **4**:  $\text{Cl}^-/\text{Br}^- \sim \text{Cl}^-/\text{I}^- > 7$ ). Considering the intrinsic overestimate with  $\text{F}^-$  (Scheme 4), O-NDI hairpin **4** emerged as a very selective chloride- $\pi$  slide (Fig. 6B and 7B, ●). The found sequence was similar to a halide VI ( $\text{Cl}^- \gg \text{F}^- \geq \text{Br}^- \sim \text{I}^-$ ). Reduced activity with both  $\text{F}^-$  and  $\text{OAc}^-$  suggested that the origin of the found chloride selectivity of dimer **4** is mainly energetic, although  $\text{F}^- > \text{OAc}^-$  may hint at contributions from size exclusion. Dominant energetics would suggest that anion binding along hairpin **4** is slightly weaker than anion binding along rod **1**, emerging sterics would agree with tighter packing of the transmembrane rods after covalent capture.

Increasing selectivity (**4** > **2** > **1**) roughly coincided with decreasing apparent activity (**1** > **2** > **4**). One possible explanation of this inverse correlation was that increasingly tight packing of transmembrane O-NDI bundles increases the selectivity of anion binding but hinders the hopping of anions from NDI to NDI. Compared to a transmembrane bundle of neutral rods **2**, the addition of positive charges to the external termini would be expected to loosen the packing of self-assembled bundles of O-NDIs **1**, whereas covalent capture in the neutral hairpin **4** would tighten the packing of O-NDIs bundles.

### Mole fraction behavior

Over the years, the HPTS assay has been adapted to the characterization of anion/cation selectivity,<sup>46,48</sup> selectivity sequences,<sup>46,48</sup> voltage-gated ion channels and pores,<sup>23,46</sup> voltage-sensitive blockage (Woodhull analysis),<sup>73</sup> synthetic catalytic pores<sup>74,75</sup> and endovesiculation.<sup>76–78,65</sup> Otherwise explored exclusively in planar bilayer conductance experiments,<sup>1–10</sup> there was no reason why the HPTS assay should not provide rapid and reliable access to mole fraction behavior of ion channels and pores in vesicles.

For this purpose, the activity of rod **1** was determined in EYPC-LUVs $\Delta$ HPTS as described above in the presence of extravascular binary mixtures of fast and slow anions. The activity of mixtures of the fast  $\text{Cl}^-$  and the slow  $\text{I}^-$  was not as high as expected from simple additivity (Fig. 9A, solid vs. dotted lines). This substantial AMFE found for  $\text{Cl}^-/\text{I}^-$  mixtures demonstrated that the transport of the two ions is competitive, and that binding of more than one  $\text{Cl}^-$  is required to observe fast transport. Moreover, close proximity of anion binding sites is required for operational charge repulsion in multiion hopping. This proximity requirement excluded decisive contributions from the otherwise quite likely additional anion binding to the Boc-Gly termini. In other words, AMFE for  $\text{Cl}^-/\text{I}^-$  mixtures provided experimental evidence for the occurrence of multiion hopping from anion- $\pi$  binding site to anion- $\pi$  binding site along rigid O-NDI rods, that is, the existence of anion- $\pi$  slides.<sup>55</sup>

AMFE was not observed in all cases. Transport of  $\text{Cl}^-/\text{ClO}_4^-$  mixtures by rod **1**, for instance, occurred with perfect additivity (Fig. 9B). This finding suggested that rod **1** almost does not transport  $\text{ClO}_4^-$ . The activities of  $\text{Cl}^-/\text{ClO}_4^-$  mixtures should

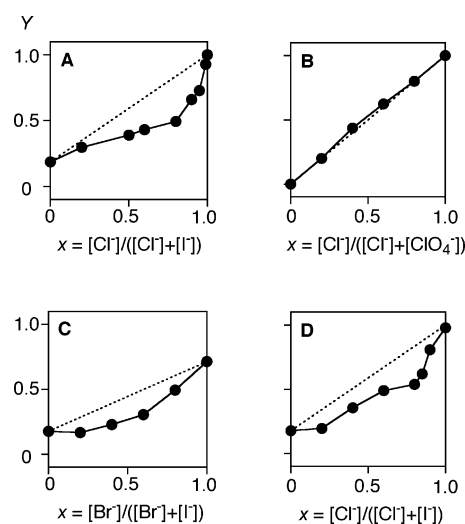


**Fig. 9** Mole fraction behavior of rod **1** (expected, dotted; found, solid) for (A)  $\text{Cl}^-/\text{I}^-$  mixtures with intravesicular  $\text{Cl}^-$ ,<sup>55</sup> (B)  $\text{Cl}^-/\text{ClO}_4^-$  mixtures with intravesicular  $\text{Cl}^-$ , (C)  $\text{Br}^-/\text{I}^-$  mixtures with intravesicular  $\text{Br}^-$  and (D)  $\text{Cl}^-/\text{I}^-$  mixtures with intravesicular  $\text{Br}^-$ . Fractional activity  $Y$  as a function of the respective mole fractions  $x$  was determined in EYPC-LUVs $\Delta$ HPTS as specified in Fig. 3.

always report on  $\text{Cl}^-/\text{OH}^-$  antiport and thus be independent of  $\text{ClO}_4^-$  concentration, which is found to be the case. (Preliminary results with similar O-NDI systems provided additional evidence for unfavorable but, different to  $\text{SO}_4^{2-}$ , still possible  $\text{ClO}_4^-$  transport.<sup>70</sup>)

The AMFE with rod **1** was also detectable for  $\text{Br}^-/\text{I}^-$  mixtures in vesicles with internal  $\text{Br}^-$  (Fig. 9C) despite the weaker discrimination between the two ions ( $\text{Br}^-/\text{I}^- = 3.0$ ,  $\text{Cl}^-/\text{I}^- = 5.0$ , Fig. 6, □). Finally, AMFE of rod **1** for  $\text{Cl}^-/\text{I}^-$  mixtures was not only detectable in vesicles with internal  $\text{Cl}^-$ , but also, although less pronounced, in vesicles with internal  $\text{Br}^-$  (Fig. 9D).

### Modeling

The cation- $\pi$  stabilizing interaction between a cation and the negative electrostatic potential on the face of an aromatic ring is a widespread phenomenon for recognition in biological and chemical systems.<sup>79,80</sup> The nature of cation- $\pi$  interactions has been studied by Dougherty *et al.*<sup>49,79–81</sup> and others.<sup>82,83</sup> They came to the conclusion that it can be described *via* the electrostatic terms. More recently it has been recognized from experimental studies in the solid state that s-triazines<sup>84</sup> and s-tetrazines<sup>85</sup> can interact favorably with anions. Other experimental studies confirmed the involvement of anion- $\pi$  binding in aromatic receptors.<sup>52,53</sup> It has been also shown by theoretical studies<sup>52–54,86</sup> that the interaction between electron deficient aromatic  $\pi$ -systems and anions is energetically favorable.

The anion- $\pi$  interaction is in general dominated by electrostatic and ion-induced polarization forces.<sup>54,86</sup> The electrostatic component of the interaction is related to the magnitude of the permanent and positive quadrupole moment ( $Q_{zz}$ ) of the aromatic system, and the anion induced polarization correlates with the molecular polarizability of the aromatic compounds.

For molecular modeling studies of rigid O-NDI rods **1–5**, the NDIs **14–18** were selected as computationally tractable model

systems (Fig. 10). The parent NDI **14** does not contain any substituents. NDIs **15** and **16** are singly N-substituted with phenyl and tetramethylphenyl spacers, respectively. NDIs **17** and **18** are doubly N-substituted with the same aryls. NDI **16** formally corresponds to the termini of O-NDIs **1–5**, and NDI **18** reproduces their central part.

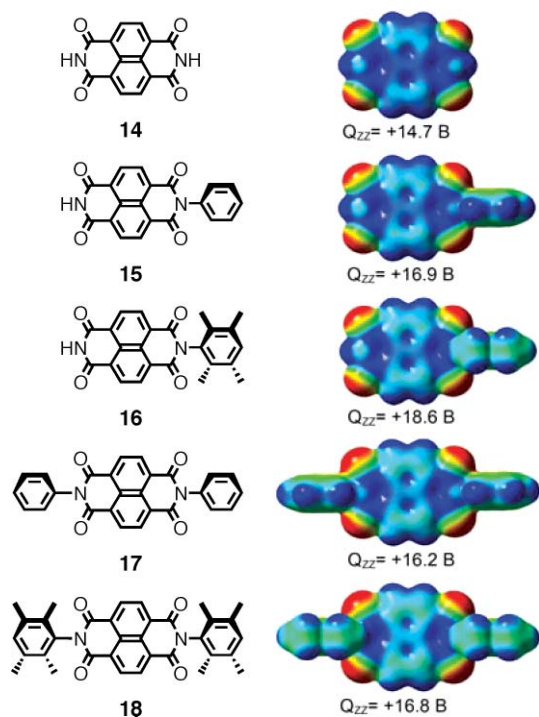


**Fig. 10** NDI model systems studied by the PBE1PBE/6-311++G\*\* method, where appropriate ( $C_s$  and  $D_{2h}$ ) symmetry was imposed. DFT computed electrostatic potential surfaces (right) are colored according to an energy scale of  $\pm 30.0$  kcal mol $^{-1}$ , where blue is positive and red is negative. Global quadrupole moments  $Q_{zz}$  in Buckingham were computed with the MP2/6-311G\*\* method.

The global quadrupole moments  $Q_{zz}$  of NDIs **14–18** were computed using the MP2/6-311G\*\*//PBE1PBE/6-311++G\*\* method. For NDI **14**,  $Q_{zz} = +14.7$  B was found. Clearly beyond the hexafluorobenzene standard ( $Q_{zz} = +9.5$  B),<sup>87</sup> the magnitude of this quadrupole moment suggested anion binding by NDI **14** would be very strong. The introduction of one or two phenyls as N-substituents further increased the  $Q_{zz}$  of NDI **15** and **17**, respectively (Fig. 10). The negative phenyl quadrupole moment produces the known  $\pi$ -basic surfaces that attract cations rather than anions.<sup>49,79,80</sup> However, the perpendicular local quadrupole moment oriented along the phenyl plane produces a  $\pi$ -acidic periphery. In DFT studies of the rotational energy profile around the NDI-phenyl single bond,<sup>88</sup> a global minimum was confirmed for the phenyl plane oriented perpendicular to the NDI plane. In this preferred conformation, the phenyl spacer reinforced the global  $Q_{zz}$  of NDI **15**, where the  $z$ -axis is perpendicular to the NDI plane. Addition of the second phenyl substituent to the other imide slightly reduced the  $Q_{zz}$  of the resulting NDI **17** (Fig. 10). A clear increase of the positive  $Q_{zz}$  was achieved by the tetramethyl substitution of the phenyl ring. Almost twice that of hexafluorobenzene, the quadrupole moment  $Q_{zz} = +16.8$  B found

for **18** is expected to reflect the situation in the central part of rigid O-NDI rods **1–5**.

Electrostatic potential surfaces provide useful indications to evaluate anion– $\pi$  interactions.<sup>89</sup> These surfaces revealed in the present case how the phenyl and tetramethylphenyl spacers modify the electrostatic environment for anion– $\pi$  interactions. Due to the perpendicular orientation of NDI and phenyl planes, the positive surface of the NDI planes of **15** and **17** extended in a continuous way to the equatorial region of the phenyl spacer. Replacement of the phenyl spacer in **15** and **17** with the tetramethylphenyl in **16** and **18** produced a more complex surface. The electrostatic potential of the methyls ranges from weakly (light blue) to distinctly positive as indicated by deep blue caps located on the hydrogens. This unique combination of electrostatic properties and conformational arrangement of NDI and tetramethylphenyl spacer produced a continuous positive surface with variable intensity of electrostatic potential. This continuous positive surface is in excellent agreement with anion hopping along rigid O-NDI rods **1–5**.

Anion binding on the NDI-surface occurred in the region of highest  $\pi$ -acidity near the imides (Fig. 11). NDI **16** was particularly well suited to study anion– $\pi$  interactions with O-NDI rigid-rods **1–5** because the two imide nitrogens differ significantly. Whereas the access to the substituent-free N1 is unrestricted, the space near N2 is confined by the tetramethylphenyl spacer. The impact of this tetramethylphenyl spacer on anion binding was investigated by moving the anion above the  $\pi$ -system while restricting it to remain in the  $C_s$  plane, which bisects the NDI moiety. The geometry parameters of anion– $\pi$  complexes **19–22** were optimized with the PBE1PBE/6-311++G\*\* method within the  $C_s$  symmetry restriction to finally obtain two minima for anions Cl $^-$  and Br $^-$  alike.

In the chloride complex **19** with the chloride in the free space near N1, the anion was found 2.95 Å above the NDI plane, the horizontal anion displacement from N1 was  $d = 1.58$  Å (Fig. 11, Table 1). In the chloride complex **20** with the chloride in the confined space near N2, the horizontal anion displacement increased to  $d = 2.16$  Å with respect to N2. The difference in horizontal anion displacement in N1 complex **19** and N2 complexes **20** indicated that steric interference from the proximal methyl in N2 complex **20** moved the chloride by 0.58 Å from the location where the optimal anion– $\pi$  interaction would occur. The resulting weakening of anion– $\pi$  interactions was further apparent in the longer distance between chloride anion and NDI plane (3.04 Å vs. 2.95 Å). The close chloride–methyl contact of 2.50 Å

**Table 1** Anion position and interaction energies with NDI **16**<sup>a</sup>

Complex <sup>b</sup>	Anion	$d/\text{Å}^c$	$\Delta d/\text{Å}^d$	$R_c/\text{Å}^e$	$E_{\text{int}}/\text{kcal mol}^{-1/f}$
<b>19</b>	Cl $^-$	1.58	—	2.95	–16.0
<b>20</b>	Cl $^-$	2.16	0.58	3.04	–18.2
<b>21</b>	Br $^-$	1.53	—	3.00	–14.0
<b>22</b>	Br $^-$	2.32	0.78	3.28	–15.7

<sup>a</sup> From PBE1PBE/6-311++G\*\* optimized geometries. <sup>b</sup> See Fig. 11.

<sup>c</sup> Horizontal anion displacement  $d$  between anion projection on the NDI plane and the nitrogen N1 (**19**, **21**) or nitrogen N2 (**20**, **22**). <sup>d</sup> Difference in horizontal anion displacement  $\Delta d$  for the same anion near N2 compared to N1. <sup>e</sup> Equilibrium distance between anion and NDI plane. <sup>f</sup> Interaction energy with BSSE correction.

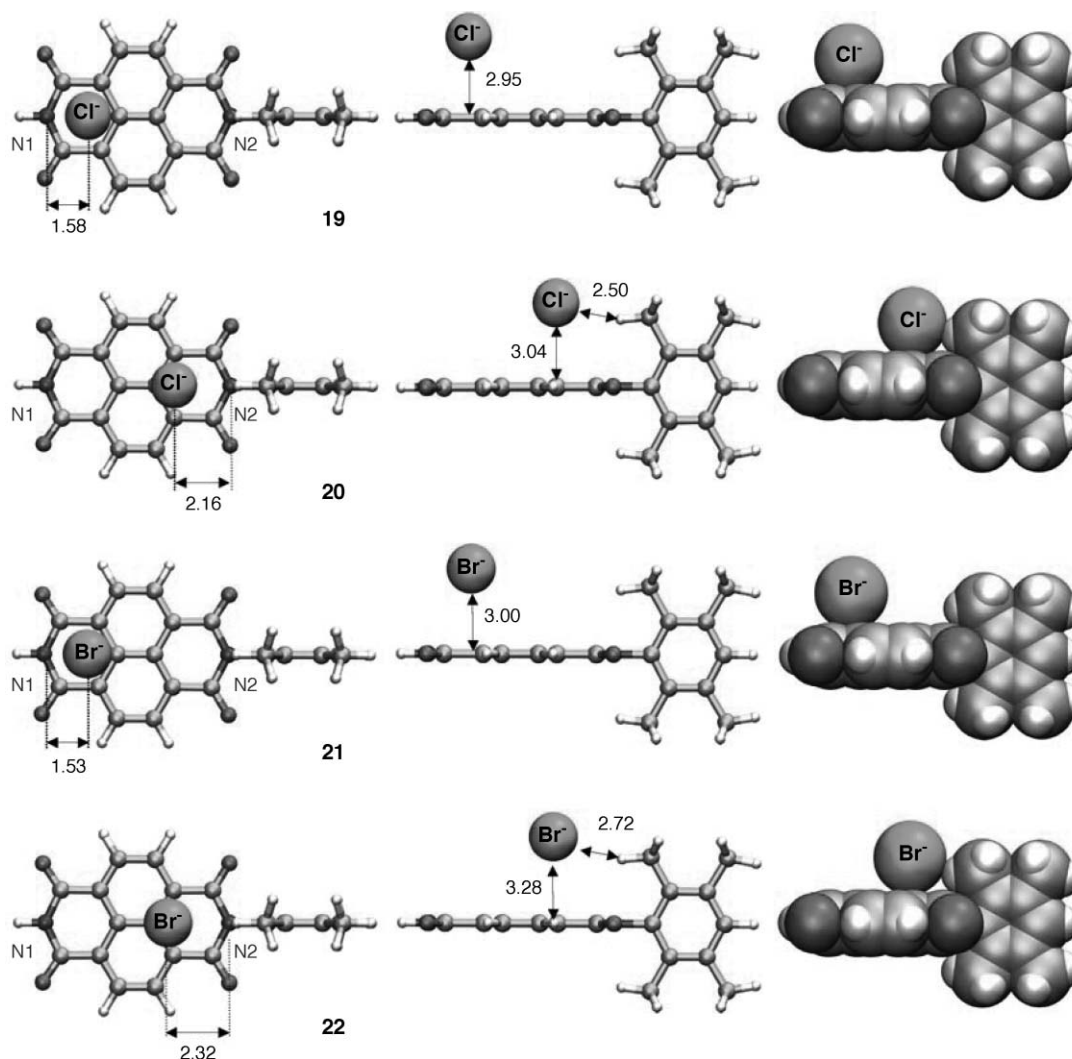


**Fig. 11** PBE1PBE/6-311++G\*\* optimized structures ( $C_s$  symmetry) of complexes **19–22** formed between NDI **16** and chloride and bromide shown in top (left) and side views (center, left) of ball and stick (atom color coding, anions green, center, left) and space filling representations (right).

supported the possibility of C–H $\cdots$ Cl $^-$  stabilizing interactions in N2 complex **20**. Similar anion–H interactions have been described, for example, in the case of linear C–H $\cdots$ X $^-$  hydrogen bonds and trifurcated CH $_3\cdots$ X $^-$  improper hydrogen bonded complexes,<sup>90,91</sup> as well as observed for anion receptors.<sup>92–94</sup>

The comparison of BSSE corrected binding energies for the two complexes **19** and **20** is of interest since they provide insight on the strength of the overall binding between the anion and model system **16**. For complex **20**, suffering from the direct interference between chloride near N2 and tetramethylphenyl spacer, the binding is stronger by 2.2 kcal mol $^{-1}$  than for interference-free association in N1 complex **19** (Table 1). This suggested that steric interference from the tetramethylphenyl spacer is largely compensated by factors such as the anion–H interaction (Fig. 11).

Comparison of chloride complexes **19** and **20** with bromide complexes **21** and **22** was of interest with regard to anion selectivity. The horizontal anion displacement for unhindered bromide binding near N1 in complex **21** was comparable to chloride binding in N1 complex **19**. The equilibrium distance from the NDI plane was only 0.05 Å longer with Br $^-$  than with

Cl $^-$ . Bromide binding in complex **22** was clearly affected by the confined space near N2. Namely, the methyl group from the spacer pushed the bromide towards the center of the NDI. The difference in horizontal anion displacement  $\Delta d = 0.78$  Å with bromide complexes was 0.20 Å beyond that found in chloride complexes (Table 1). Moreover, the distance  $R_c = 3.28$  of the bromide from the NDI plane in the N2 complex **22** was 0.24 Å longer than that of chloride in the N2 complex **20**. Both effects suggested that the spatial confinement imposed by tetramethylphenyl spacers may provide access to anion– $\pi$  slides with selectivity for small anions. Similar to the N2 chloride complex **20**, the N2 bromide complex **22** revealed a close contact of 2.72 Å between Br $^-$  and CH $_3$ . The energy found for bromide binding in the confined space near N2 in complex **22** was 1.7 kcal mol $^{-1}$  higher than that for unhindered bromide binding near N1 in complex **21**. This was only 0.5 kcal mol $^{-1}$  less than the energy gains for chloride binding in the confined N2 region in complex **20**.

Insights from molecular modeling thus not only confirmed the possibility of anion binding on the  $\pi$ -acidic NDI surfaces but also revealed preferential anion interaction near the imide

nitrogen. Advanced binding sites in confined spaces produced by the methyl substituents on the phenyl spacer were found to contribute more to anion binding (1.7–2.2 kcal mol<sup>-1</sup>) than to Cl<sup>-</sup> > Br<sup>-</sup> selectivity (0.5 kcal mol<sup>-1</sup>). In general, these findings are in excellent qualitative agreement with experimental results. Possibly more important effects with larger anions as well as correlations with desolvation penalties<sup>49</sup> remain to be explored. Moreover, spacer engineering can be formulated as an attractive rational approach to the design of advanced anion- $\pi$  slides.

With the only intention to generate a feeling for possible active suprastructures, various parallel tetrameric bundles of asymmetric O-NDI rod **2** were loaded with three chloride anions and subjected to short molecular dynamics simulations *in vacuo* (Fig. 12). O-NDI bundles **23** display longitudinal displacement of anion- $\pi$  slides to produce a string of aligned aromatic binding sites. Each site is composed of two face-to-face oriented NDIs and two tetramethylphenyls. Adjacent aromatic rings are naturally rotated by 90°. The terminal binding sites in bundles **23**, composed of two NDI and two glycine termini, each revealed possible contributions from the mildly acidic amide, carbamate, amine and ammonium hydrogens in the latter. Preliminary computational studies suggested that these terminal functional groups may be able to act as isolate anion receptors on their own and thus provide an attractive additional end-group engineering approach<sup>23,24</sup> to refine the anion selectivity of O-NDI rods. However, significant contributions from end-group engineering to multiion hopping and anion selectivity were not supported by AMFE results, preliminary results indicated preserved anion selectivity of rigid-rod  $\pi$ -slides with tetraanionic end groups. More generally, we caution that these preliminary models of possible active suprastructures were obtained under highly simplified conditions far from reality (excluding, *e.g.*, surrounding membrane and explicit water). They were prepared with the only intention to more qualitatively assist

the visualization of the rich complexity encountered in active O-NDI suprastructures and must be considered with appropriate caution.

## Summary and conclusion

A small collection of rigid oligo-*p*-phenylene-*N,N*-naphthalenediimide (O-NDI) rods was synthesized to elaborate on the formation and nature of transmembrane anion- $\pi$  slides for multiion hopping across lipid bilayer membranes. According to the HPTS assay in EYPC vesicles, rods with one charged terminus have the highest activity, whereas the activity of rods with charges at both termini was weaker than that of uncharged rods. These trends suggested that transmembrane rod orientation is needed for activity. Hill plots were in support of either exergonic self-assembly into active suprastructures or monomeric active structures.

The most active cationic O-NDI rods (**2**) exhibited a rather weak (Cl<sup>-</sup>/I<sup>-</sup> = 1.9) selectivity similar to a halide IV topology (Cl<sup>-</sup> > Br<sup>-</sup> > I<sup>-</sup> > F<sup>-</sup>). This selectivity increased to a more pronounced (Cl<sup>-</sup>/I<sup>-</sup> = 7.6) and quite unusual halide VI topology with the less active neutral O-NDI rods (**1**, Cl<sup>-</sup> > F<sup>-</sup> > Br<sup>-</sup> > I<sup>-</sup>). Covalent capture as rigid-rod O-NDI hairpins gave neutral anion- $\pi$  slides (**4**) with poor activity but excellent chloride selectivity (Cl<sup>-</sup>/I<sup>-</sup> ~ Cl<sup>-</sup>/Br<sup>-</sup> > 7). These trends suggested that proximity of transmembrane rods is required for both activity and selectivity, the former decreasing and the latter increasing with increasing lateral rod proximity. Selective transport of anions with high hydration energy suggested strong anion binding along the anion- $\pi$  slides. Similar selectivity for F<sup>-</sup> and OAc<sup>-</sup> supported dominant energetics and excluded significant contributions from size exclusion. The pronounced chloride selectivity of O-NDI hairpin **4** implied slightly decreasing importance of energetics and increasing of contributions from size exclusion (F<sup>-</sup> > OAc<sup>-</sup>).

Lower than expected activity of mixtures of Cl<sup>-</sup>/I<sup>-</sup> and Br<sup>-</sup>/I<sup>-</sup> but not Cl<sup>-</sup>/ClO<sub>4</sub><sup>-</sup> demonstrated that more than one binding site in close proximity is required for fast transport. These significant AMFEs thus confirmed the existence of anion- $\pi$  slides, *i.e.*, multiion hopping along the rigid O-NDI rods across the bilayer membrane.

With a significant inverted quadrupole moment of at least +14.7 B, almost twice that of hexafluorobenzene (+8.9 B) and beyond that of significant negative counterparts such as pyrene (-13.8 B), *ab initio* and DFT calculations confirmed the potential of NDIs for anion- $\pi$  interactions. Molecular models further highlighted the role of the four methyl groups in the phenyl spacers to reduce the available size of the  $\pi$ -acidic centers of the NDI surface for perfect accommodation of small anions such as chloride or bromide, and to magnify the NDI quadrupole moment.

The remarkable consistence of the found characteristics with operational anion- $\pi$  slides should not distract from the fact that many aspects of introduced concept remain highly speculative. Several interpretations and conclusions made may thus be best considered as tentative, made with the only intention to stimulate progress in the field. Current efforts to synthesize advanced anion- $\pi$  slides focus on hydrophilic anchoring to increase overall activity,<sup>70</sup> on varied substitution patterns on the phenyl spacers and the NDI core,<sup>62</sup> and on varied positioning of the NDI acceptors along the rigid-rod scaffold.

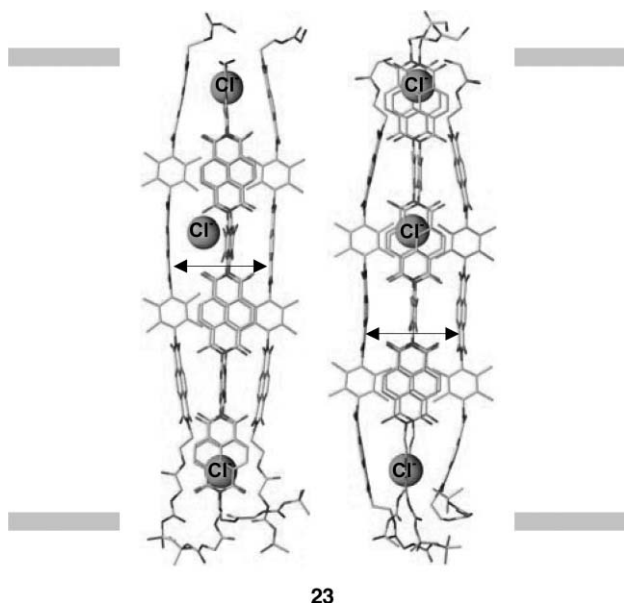


**Fig. 12** Optimized geometry of a notional active suprastructure after a molecular dynamics simulation of 1500 ps *in vacuo*, that is, tetramer **23**, formed by four parallel monomers **2** (amine terminus up, Boc terminus down) and loaded with three chlorides (green). The indicated NDI-NDI distances (arrows) are 9.55 Å (left) and 8.35 Å (right).

## Acknowledgements

We thank D. Jeannerat, A. Pinto and S. Grass for NMR measurements, P. Perrottet and the group of F. Gülaçar for ESI MS measurements, N. Oudry and G. Hopfgartner for MALDI MS measurements, CSCS in Manno for CPU time on their CRAY-XT3 and IBM Power5-575 computers, P. Tecilla (Trieste) and both referees for very helpful suggestions, and the Swiss NSF for financial support.

## References

- 1 B. Hille and W. Schwarz, *J. Gen. Physiol.*, 1978, **72**, 409–442.
- 2 C. Miller, *J. Gen. Physiol.*, 1999, **113**, 783–787.
- 3 G. Eisenman and R. Horn, *J. Membr. Biol.*, 1983, **76**, 197–225.
- 4 E. M. Wright and J. M. Diamond, *Physiol. Rev.*, 1977, **57**, 109–156.
- 5 J. A. Tabcharani, J. M. Rommens, Y.-X. Hou, X.-B. Chang, L.-C. Tsui, J. R. Riordan and J. W. Hanrahan, *Nature*, 1993, **366**, 79–82.
- 6 P. Lindsell, *J. Physiol.*, 2001, **531**, 51–66.
- 7 P. Lindsell, *Exp. Physiol.*, 2006, **91**, 123–129.
- 8 M. Pusch, U. Ludewig, A. Rehfeldt and T. J. Jentsch, *Nature*, 1995, **373**, 527–531.
- 9 Z. Qu and H. C. Hartzell, *J. Gen. Physiol.*, 2000, **116**, 825–884.
- 10 M. Duszynk, D. Liu, A. S. French and S. F. Man, *Eur. Biophys. J.*, 1993, **22**, 5–11.
- 11 U. Zachariae, V. Helms and H. Engelhardt, *Biophys. J.*, 2003, **85**, 954–962.
- 12 R. Dutzler, E. B. Campbell and R. MacKinnon, *Science*, 2003, **300**, 108–112.
- 13 D. A. Doyle, J. M. Cabral, R. A. Pfuetzner, A. Kuo, J. M. Gulbis, S. L. Cohen, B. T. Chait and R. MacKinnon, *Science*, 1998, **280**, 69–77.
- 14 R. Dutzler, *FEBS Lett.*, 2004, **564**, 229–233.
- 15 A. P. Davis, D. N. Sheppard and B. D. Smith, *Chem. Soc. Rev.*, 2007, **36**, 348–357.
- 16 P. Scrimin and P. Tecilla, *Curr. Opin. Chem. Biol.*, 1999, **3**, 730–735.
- 17 G. W. Gokel and A. Mukhopadhyay, *Chem. Soc. Rev.*, 2001, **30**, 274–286.
- 18 T. M. Fyles, *Chem. Soc. Rev.*, 2007, **36**, 335–347.
- 19 S. Matile, A. Som and N. Sordé, *Tetrahedron*, 2004, **60**, 6405–6435.
- 20 A. L. Sisson, M. R. Shah, S. Bhosale and S. Matile, *Chem. Soc. Rev.*, 2006, **35**, 1269–1286.
- 21 M. Yoshii, M. Yamamura, A. Satake and Y. Kobuke, *Org. Biomol. Chem.*, 2004, **2**, 2619–2623.
- 22 Y. J. Jeon, H. Kim, S. Jon, N. Selvapalam, D. Y. Oh, I. Seo, C.-S. Park, S. R. Jung, D.-S. Koh and K. Kim, *J. Am. Chem. Soc.*, 2004, **126**, 15944–15945.
- 23 N. Sakai, D. Gerard and S. Matile, *J. Am. Chem. Soc.*, 2001, **123**, 2517–2524.
- 24 P. L. Boudreault and N. Voyer, *Org. Biomol. Chem.*, 2007, **5**, 1459–1465.
- 25 J. R. Pfeifer, P. Reiss and U. Koert, *Angew. Chem., Int. Ed.*, 2006, **45**, 501–504.
- 26 N. Sakai, N. Sordé, G. Das, P. Perrottet, D. Gerard and S. Matile, *Org. Biomol. Chem.*, 2003, **1**, 1226–1231.
- 27 M. Suzuki, T. Morita and T. Iwamoto, *Cell. Mol. Life Sci.*, 2006, **63**, 12–24.
- 28 J. R. Broughman, L. P. Shank, W. Takeguchi, B. D. Schultz, T. Iwamoto, K. E. Mitchell and J. M. Tomich, *Biochemistry*, 2002, **41**, 7350–7358.
- 29 G. Deng, T. Dewa and S. L. Regen, *J. Am. Chem. Soc.*, 1996, **118**, 8975–8976.
- 30 C. W. Jiang, E. R. Lee, M. B. Lane, Y. F. Xiao, D. J. Harris and S. H. Cheng, *Am. J. Physiol.: Lung Cell. Mol. Physiol.*, 2001, **281**, L1164.
- 31 R. Pajewski, R. Ferdani, J. Pajewska, N. Djedovic, P. H. Schlesinger and G. W. Gokel, *Org. Biomol. Chem.*, 2005, **3**, 619–625.
- 32 B. Ding, N. Yin, Y. Liu, J. Cardenas-Garcia, R. Evanson, T. Orsak, M. Fan, G. Turin and P. B. Savage, *J. Am. Chem. Soc.*, 2004, **126**, 13642–13648.
- 33 B. Ding, U. Taotofa, T. Orsak, M. Chadwell and P. B. Savage, *Org. Lett.*, 2004, **6**, 3433–3436.
- 34 R. F. Epand, T. L. Raguse, S. H. Gellman and R. M. Epand, *Biochemistry*, 2004, **43**, 9527–9535.
- 35 J. A. Patch and A. E. Barron, *J. Am. Chem. Soc.*, 2003, **125**, 12092–12093.
- 36 M. F. Ilker, K. Nüsslein, G. N. Tew and E. B. Coughlin, *J. Am. Chem. Soc.*, 2004, **126**, 15870–15875.
- 37 J. Rennie, L. Arnt, H. Tang, K. Nüsslein and G. N. Tew, *J. Ind. Microbiol. Biotechnol.*, 2005, **32**, 296–300.
- 38 J. L. Sessler, L. R. Eller, W. S. Cho, S. Nicolaou, A. Aguilar, J. T. Lee, V. M. Lynch and D. J. Magda, *Angew. Chem., Int. Ed.*, 2005, **44**, 5989–5992.
- 39 P. A. Gale, *Acc. Chem. Res.*, 2006, **39**, 465–475.
- 40 V. Sidorov, F. W. Kotch, G. Abdrakhmanova, R. Mizani, J. C. Fettingler and J. T. Davis, *J. Am. Chem. Soc.*, 2002, **124**, 2267–2278.
- 41 J. L. Seganish, J. C. Fettingler and J. T. Davis, *Supramol. Chem.*, 2006, **18**, 257–264.
- 42 P. V. Santacrose, O. A. Okunola, P. Y. Zavalij and J. T. Davis, *Chem. Commun.*, 2006, **41**, 3246–3248.
- 43 B. A. McNally, A. V. Koulov, B. D. Smith, J. B. Joos and A. P. Davis, *Chem. Commun.*, 2005, **41**, 1087–1089.
- 44 J. P. Clare, A. J. Ayling, J. B. Joos, A. L. Sisson, G. Magro, M. N. Pérez-Payán, T. N. Lambert, R. Shukla, B. D. Smith and A. P. Davis, *J. Am. Chem. Soc.*, 2005, **127**, 10739–10746.
- 45 N. Madhavan, E. C. Robert and M. S. Gin, *Angew. Chem., Int. Ed.*, 2005, **44**, 7584–7587.
- 46 N. Sakai, D. Houdebert and S. Matile, *Chem.–Eur. J.*, 2003, **9**, 223–232.
- 47 Y. Tanaka, Y. Kobuke and M. Sokabe, *Angew. Chem., Int. Ed. Engl.*, 1995, **34**, 693–694.
- 48 M. M. Tedesco, B. Ghebremariam, N. Sakai and S. Matile, *Angew. Chem., Int. Ed.*, 1999, **38**, 540–543.
- 49 R. A. Kumpf and D. A. Dougherty, *Science*, 1993, **261**, 1708–1710.
- 50 R. M. Fairchild and K. T. Holmann, *J. Am. Chem. Soc.*, 2005, **127**, 16364–16365.
- 51 Y. S. Rosokha, S. V. Lindeman, S. V. Rosokha and J. K. Kochi, *Angew. Chem., Int. Ed.*, 2004, **43**, 4650–4652.
- 52 M. Mascal, A. Armstrong and M. D. Bartberger, *J. Am. Chem. Soc.*, 2002, **124**, 6274–6276.
- 53 I. Alkorta, I. Rozas and J. Elguero, *J. Am. Chem. Soc.*, 2002, **124**, 8593–8598.
- 54 C. Garau, D. Quiñonero, A. Frontera, P. Ballester, A. Costa and P. M. Deyà, *J. Phys. Chem. A*, 2005, **109**, 9341–9345.
- 55 V. Gorteau, G. Bollot, J. Mareda, A. Perez-Velasco and S. Matile, *J. Am. Chem. Soc.*, 2006, **128**, 14788–14789.
- 56 L. L. Miller, B. Zinger and J. S. Schlechte, *Chem. Mater.*, 1999, **11**, 2313–2315.
- 57 D.-S. Choi, Y. S. Chong, D. Whitehead and K. D. Shimizu, *Org. Lett.*, 2001, **3**, 2757–2760.
- 58 J. Gawronski and K. Kacprzak, *Chirality*, 2002, **14**, 689–702.
- 59 J. Lee, V. Guelev, S. Sorey, D. W. Hoffman and B. L. Iverson, *J. Am. Chem. Soc.*, 2004, **126**, 14036–14042.
- 60 S. A. Vignon, T. Jarrosson, T. Iijima, H. R. Tseng, J. K. M. Sanders and J. F. Stoddart, *J. Am. Chem. Soc.*, 2004, **126**, 9884–9885.
- 61 P. Mukhopadhyay, Y. Iwashita, M. Shirakawa, S. Kawano, N. Fujita and S. Shinkai, *Angew. Chem., Int. Ed.*, 2006, **45**, 1592–1595.
- 62 S. Bhosale, A. L. Sisson, P. Talukdar, A. Fürstenberg, N. Banerji, E. Vauthey, G. Bollot, J. Mareda, C. Röger, F. Würthner, N. Sakai and S. Matile, *Science*, 2006, **313**, 84–86.
- 63 B. Ghebremariam, V. Sidorov and S. Matile, *Tetrahedron Lett.*, 1999, **40**, 1445–1448.
- 64 C. Ni and S. Matile, *Chem. Commun.*, 1998, **33**, 755–756.
- 65 S. Matile and N. Sakai, *The Characterization of Synthetic Ion Channels and Pores*, in Analytical Methods in Supramolecular Chemistry, ed. C. A. Schalley, Wiley, Weinheim, 2007, pp. 391–418.
- 66 S. Litvinchuk, G. Bollot, J. Mareda, A. Som, D. Ronan, M. R. Shah, P. Perrottet, N. Sakai and S. Matile, *J. Am. Chem. Soc.*, 2004, **126**, 10067–10075.
- 67 A. V. Hill, *Biochem. J.*, 1913, **7**, 471–480.
- 68 S. Bhosale and S. Matile, *Chirality*, 2006, **18**, 849–856.
- 69 N. Sakai and S. Matile, *J. Phys. Org. Chem.*, 2006, **19**, 452–460.
- 70 V. Gorteau, A. Perez-Velasco and S. Matile, in preparation.
- 71 N. Sakai, Y. Kamikawa, M. Nishii, T. Matsuoka, T. Kato and S. Matile, *J. Am. Chem. Soc.*, 2006, **128**, 2218–2219.
- 72 D. Ronan, N. Sordé and S. Matile, *J. Phys. Org. Chem.*, 2004, **17**, 978–982.
- 73 Y. Baudry, D. Pasini, M. Nishihara, N. Sakai and S. Matile, *Chem. Commun.*, 2005, **40**, 4798–4800.
- 74 B. Baumeister, N. Sakai and S. Matile, *Org. Lett.*, 2001, **3**, 4229–4232.
- 75 N. Sakai, N. Sordé and S. Matile, *J. Am. Chem. Soc.*, 2003, **125**, 7776–7777.

- 76 M. Tedesco and S. Matile, *Bioorg. Med. Chem.*, 1999, **7**, 1373–1379.
- 77 H. Matsuo, J. Chevallier, F. Vilbois, R. Sadoul, J. Fauré, S. Matile, N. Sartori Blanc, J. Dubochet and J. Gruenberg, *Science*, 2004, **303**, 531–534.
- 78 C. A. Winschel, A. Kalidindi, I. Zgani, J. L. Magruder and V. Sidorov, *J. Am. Chem. Soc.*, 2005, **127**, 14704–14713.
- 79 D. A. Dougherty, *Science*, 1996, **271**, 163–168.
- 80 J. C. Ma and D. A. Dougherty, *Chem. Rev.*, 1997, **97**, 1303–1324.
- 81 J. P. Gallivan and D. A. Dougherty, *J. Am. Chem. Soc.*, 2000, **122**, 870–874.
- 82 E. Cubero, F. J. Luque and M. Orozco, *Proc. Natl. Acad. Sci. U. S. A.*, 1998, **95**, 5976–5980.
- 83 S. Tsuzuki, M. Yoshida, T. Uchimaru, M. Mikami and K. Tanabe, *J. Phys. Chem. A*, 2001, **105**, 769–773.
- 84 S. Demeshko, S. Dechert and F. Meyer, *J. Am. Chem. Soc.*, 2004, **126**, 4508–4509.
- 85 B. L. Schottel, H. T. Chifotides, M. Shatruk, A. Chouai, L. M. Pérez, J. Bacsá and K. R. Dunbar, *J. Am. Chem. Soc.*, 2006, **128**, 5895–5912.
- 86 C. Garau, A. Frontera, D. Quiñero, P. Ballester, A. Costa and P. M. Deyà, *ChemPhysChem*, 2003, **4**, 1344–1348.
- 87 J. Hernandez-Trujillo and A. Vela, *J. Phys. Chem.*, 1996, **100**, 6524–6530.
- 88 G. Bollot, V. Gorteau, S. Matile and J. Mareda, in preparation.
- 89 D. L. Beene, G. S. Brandt, W. Zhong, N. M. Zacharias, H. A. Lester and D. A. Dougherty, *Biochemistry*, 2002, **41**, 10262–10269.
- 90 P. Hobza and Z. Havlas, *Chem. Rev.*, 2000, **100**, 4253–4264.
- 91 E. S. Kryachko and T. Zeegers-Huyskens, *J. Phys. Chem. A*, 2002, **106**, 6832–6838.
- 92 K. I. Nattinen and K. Rissanen, *CrystEngComm*, 2003, **5**, 326–330.
- 93 S. J. Coles, J. G. Frey, P. A. Gale, M. B. Hursthouse, M. E. Light, K. Navakhun and G. L. Thomas, *Chem. Commun.*, 2003, 568–569.
- 94 E. Light, P. A. Gale and K. Navakhun, *Acta Crystallogr., Sect. E: Struct. Rep. Online*, 2006, **62**, 1097–1098.